



HAL
open science

Role of inclusions, surface roughness and operating conditions on rolling contact fatigue

Daniel Nélias, Jean-Michel Dumont, F. Champiot, A. Vincent, Daniel Girodin, Louis Flamand

► **To cite this version:**

Daniel Nélias, Jean-Michel Dumont, F. Champiot, A. Vincent, Daniel Girodin, et al.. Role of inclusions, surface roughness and operating conditions on rolling contact fatigue. *Journal of Tribology*, 1999, 121 (2), pp.240-251. 10.1115/1.2833927 . hal-04713957

HAL Id: hal-04713957

<https://hal.science/hal-04713957v1>

Submitted on 2 Jan 2025

HAL is a multi-disciplinary open access archive for the deposit and dissemination of scientific research documents, whether they are published or not. The documents may come from teaching and research institutions in France or abroad, or from public or private research centers.

L'archive ouverte pluridisciplinaire **HAL**, est destinée au dépôt et à la diffusion de documents scientifiques de niveau recherche, publiés ou non, émanant des établissements d'enseignement et de recherche français ou étrangers, des laboratoires publics ou privés.

Role of Inclusions, Surface Roughness and Operating Conditions on Rolling Contact Fatigue

D. Nélias, M. L. Dumont¹

Laboratoire de Mécanique des Contacts, CNRS UMR 5514, INSA de Lyon, 20 Av. A. Einstein, 69621 Villeurbanne Cedex, France

F. Champiot, A. Vincent

G.E.M.P.P.M., CNRS UMR 5510, INSA de Lyon, 20 Av. A. Einstein, 69621 Villeurbanne Cedex, France

D. Girodin

SNR Roulements, BP 2017, 74010 Annecy, France

R. Fougères

G.E.M.P.P.M. CNRS UMR 5510, INSA de Lyon, 20 Av. A. Einstein, 69621 Villeurbanne Cedex, France

L. Flamand

Laboratoire de Mécanique des Contacts, CNRS UMR 5514, INSA de Lyon, 20 Av. A. Einstein, 69621 Villeurbanne Cedex, France

Tests have been performed on a two-disk machine in order to evaluate the role of inclusions, surface roughness and operating conditions on rolling contact fatigue of AISI 52100 and M50 bearing steels. Important parameters—such as nature and location of inclusions, small and large wavelengths of surface roughness, normal loading or sliding conditions—on crack initiation and propagation stages have been identified. The operating conditions have been selected to encompass typical jet engine applications. Tests have been carried out up to 4.2 GPa, for two different surface finishes. Surface distress and sub-surface damage which could result in catastrophic failure have been observed. Indeed, surface initiated deep spalling (observed at 3.5 GPa for unpolished surfaces and under rolling plus sliding conditions) as well as sub-surface initiated deep spalling (at 4.2 GPa for polished specimens) have been observed. Sub-surface micro-cracks were detected early and followed during some interrupted tests by the means of an ultrasonic echographic device. Results of our experiments are analyzed and discussed in relation to the rolling contact fatigue theories.

Introduction

From a general point of view, the rolling contact fatigue phenomenon is induced by the cyclic loading of contacting surfaces at low sliding ratios. Other damage, like wear or scuffing, may occur under extreme operating conditions. Wear appears at a microscopic scale under high tangential stresses in the contact area (Clarke et al., 1985). Scuffing occurs at high sliding rates under high thermal and tangential shear stresses and involves local welding or adhesion (Dyson, 1975). The context of rolling contact fatigue (R.C.F.) does not include high sliding and therefore thermal effects.

The process of rolling contact fatigue is commonly divided in two steps:

The first one is the initiation or nucleation of micro-cracks due to the local accumulation of dislocations within the contacting bodies. This step is initially due to the concentration of high local stresses and associated plastic deformation around sub-surface inhomogeneities or surface defects, which both act

as stress raisers. One can see, for example, the experimental investigations on inclusion originated fatigue (Littmann et al., 1966; Martin et al., 1967; Littmann, 1970; Yoshioka et al., 1988, 1993, and 1995), and on surface crack initiation around artificially produced defects (Cheng et al., 1994a and 1994b) or debris indentation (Averbach et al., 1991).

The second one is the slow growth of the micro-cracks until the fracture toughness of the material is reached and surface distress is observed—also called micro-pitting or peeling—(Berthe, 1978; Soda et al., 1982; Cheng et al., 1995; Nélias et al., 1998; Chiu, 1998), or deep spalling appears (Way, 1935; Littmann et al., 1966; Littmann, 1970; Yoshioka, 1988; Tallian, 1992).

In fact, R.C.F. is a complex phenomenon influenced by the material properties, the contact geometry, the kinematics, the loading, the lubricant properties, the temperature and the surface topography which can generate local stress distributions in the material. As a function of these parameters, two main types of R.C.F. are well identified, depending on their size (Tallian, 1992):

- Deep spalling, due to the formation of a contact-scale spall. A spall can be either surface or sub-surface initiated.
- Surface distress, made of a large population of asperity-scale micro-spalls and micro-cracks. A distinction should be made between surface distress produced under pure rolling condi-

¹ Currently at SKF Engineering and Research Centre, Nieuwegein, The Netherlands.

tions—made mainly of micro-spalls—and that observed under rolling plus sliding, which is made of wider micro-spalls with transverse micro-cracks (Nélias et al., 1998).

The purposes of this experimental study are:

- To identify the mechanisms of surface and sub-surface originated fatigue occurring in elastohydrodynamically lubricated contacts, like those found in rolling bearings and gears,
- to evaluate the important parameters of rolling contact fatigue initiation and propagation steps,
- to provide experimental data to validate a model of crack initiation and propagation in elastohydrodynamically lubricated contacts. This part of the work will be presented later in a future paper.

State of Art on Sub-Surface or Surface Initiated R.C.F.

First of all, it should be mentioned that, although modeling is often supported by some experimental investigations, most of the work published on R.C.F. is theoretical.

Although the prediction of R.C.F. still depends strongly on empirical methods originated from the outstanding work of Lundberg and Palmgren (1947), the analysis based on the micromechanics of crack initiation and propagation using the dislocation theory is a more physically satisfying and rational approach. Among the many studies in this area is the pioneering work on crack initiation of Mura and his co-workers (1981; 1990); Tanaka et al. (1982); Champaud (1988); Zhou et al. (1989); and more recently of Sanchette-Gosset (1993), Cheng et al. (1994c; 1997); Lamagnère (1996); and Vincent et al. (1997). Modeling of crack propagation under rolling contact fatigue has been extensively studied by Keer et al. (1983); Murakami et al. (1985 and 1994); Zhou et al. (1989); Fan et al. (1993); Rocher (1994); Kuo et al. (1997); Lee et al. (1997); and Champiot (1997).

Sites and modes of fatigue crack initiation depend on the cleanliness and microstructure of the material, normal and tangential loading, and micro-geometry of the contacting surfaces. It is well-known that micro-cracks can be initiated along slip bands by dislocation motion, along grain boundaries, along interfaces of inclusions or around voids or other inhomogeneities within the material. Mura and Tanaka (1981) have proposed a model for crack initiation in homogeneous media or starting at inclusions. This model has been recently improved by Champaud (1988), Sanchette-Gosset (1993) and Lamagnère (1996) and finally applied to define conditions for infinite life of bearings (Lamagnère et al., 1998).

Vincent et al. (1995) have modeled the three-dimensional shape of a butterfly formed around a given inclusion in bearing steel under R.C.F.. The stress raiser effect of a single or multiple inclusions is nicely presented by Sushchenko (1997), which simulates photoelastically the stress concentration at the interface between hard inclusions and a metal matrix, using a two-dimensional polymer model with polymer inclusions of higher elastic modulus.

Following the nucleation stage, fatigue cracks could either propagate or be stopped. Sub-surface cracks may stop growing if their length is below a critical value, depending on the cyclic loading and its location below the contact. There is considerable experimental and analytical evidence indicating an arrest region for the crack growth from or towards the Hertzian depth. This arrest region is better known as the quiescent zone, as postulated by Tallian et al. (1978). That contributes to explain why some cracks may not propagate and some others do, crossing this zone between the near-surface and the Hertzian depth due to asperity, surface friction or inclusion-driving effects (Clarke et al., 1985; Blake and Cheng, 1991).

A three-dimensional crack propagation model was presented by Lee and Keer (1986). Refinements including interactions

between multiple cracks or inclusions have been introduced recently by Kuo et al. (1997) and Lee et al. (1997).

Concerning lubricant action, it is now well accepted that the oil hydraulic pressure effect pointed out by Way in 1935 is a possible mechanism of surface crack growth. The theoretical work carried out by Kaneta et al. (1985), Murakami et al. (1985, 1994), and Bower (1988) tends to clarify the role of lubricant on surface crack propagation due to the oil hydraulic pressure action. The oil viscosity seems to be an important factor as it governs the amount of oil entrapped within the crack cavity (Litmann et al., 1968). The oil also plays a role on R.C.F. by its lubricating action on the crack faces, by the additives it contains and through the foreign particles that it carries and which may dent the contacting surfaces (Matsuo et al., 1994, Shibata et al., 1994).

The statistical distribution of the fatigue life using micro-mechanics modeling of crack initiation and propagation was also obtained by Meynaud et al. (1995a, 1995b), assuming a statistical distribution of inclusion size, nature, and depth within the material. This model shows that the semi-empirical approach of Lundberg and Palmgren, based on continuum mechanics theory, is no longer required to correlate experimental data and numerical results.

As one can see, the process of rolling contact fatigue induces complex phenomena, including many modes and sites of crack nucleation, a wide range of factors affecting crack growth, and competitive modes of crack propagation and wear. Additional experimental work is then required in order to identify mechanisms of R.C.F. as well as dominant parameters.

Experimental Procedure

Test Rig and Operating Conditions. Fatigue tests have been carried out on a high-speed twin-disk machine, described elsewhere by Nélias et al. (1998). This simulator reproduces the operating conditions of high-speed rolling bearings at the raceway-rolling element contact, i.e., rolling and sliding speeds, contact pressure, lubricant, temperature, material, and surface finish. It should be noted that the shape of the disk specimens has been chosen spherical for these experiments, in such a manner that the contact conjunction is circular (Fig. 1). The lubricant used is a tetra-ester of 5 cst viscosity at 100°C, qualified for use in gas turbine engine lubrication systems under the MIL-L-23699 specifications. The oil jet temperature was maintained constant at 80°C during all tests, which is also the bulk temperature of the tested disks due to the abundant oil flow. Tribological and rheological properties of this lubricant are described elsewhere by Vergne et al. (1996).

Tests have been carried out for two rolling bearing steels (AISI 52100 and M50), two surface roughnesses (grinding with and without polishing, respectively $R_a \approx 0.1 \mu\text{m}$ and $R_a \approx 0.5 \mu\text{m}$), three normal loadings (1.5, 2.5, and 3.5 GPa) and under pure rolling and rolling plus sliding conditions. Tests have been carried out for pairs of disks either both smooth (i.e., grinding with polishing) or both rough (i.e., without polishing). The mean contact velocity is set equal to 40 m/s for each test. To avoid thermal effects and scuffing, the slide-to-roll ratio $s = (u_1 - u_2)/(u_1 + u_2)$ has been chosen equal to 0.06, 0.035, and 0.02, respectively, at 1.5, 2.5, and 3.5 GPa. An additional test has been performed at 4.2 GPa under pure rolling, for M50 specimens with polished surfaces, and a mean contact velocity of 30 m/s. The list of tests is given in Appendix A.

The hardness ranges from 58 to 61 Rc and from 62 to 64 Rc for the 52100 and the M50 steels, respectively. The tempering temperature was 240°C and 550°C for the 52100 and the M50 steels, respectively. Residual stress profiles measured by X-ray diffraction show that grinding and polishing produce compressive residual stresses in a thin layer of about 5 μm only. Indeed, the mean residual stresses measured on the disk surfaces were -200 and -300 MPa for the 52100 steel, -300 and -400 MPa

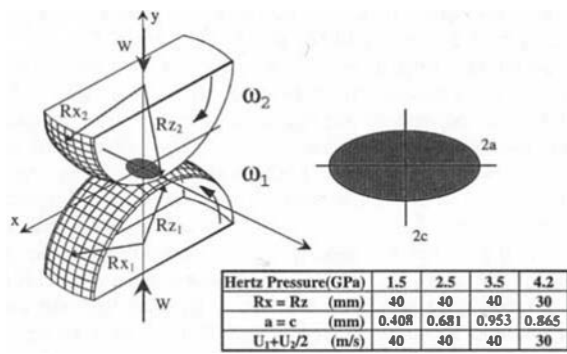


Fig. 1 Contact geometry

for the M50 steel, without and with polishing, respectively. Moreover, the influence of polishing is significant (about 100 MPa) both for 52100 and M50. More details on the measured surface profiles before and after running and on the subsequent elastic stress field are given by Dumont (1997).

High Frequency Ultrasonic Echography. The high frequency ultrasonic echography allows one to get an early detection of sub-surface cracks and to follow their possible propagation up to the surface. Since the scanning echography technique is time consuming and it requires that the fatigue tests are interrupted in order to enable the disk specimens to be examined, only a few selected tests were carried out by using this technique.

Ultrasonic methods are well known to be used for Non Destructive Testing (N.D.T.) purposes. However, because of the very small size (20 to 30 μm) of the possible initiation sites constituted by the inclusions and primary carbides, and then by micro-cracks, a very well focused beam has to be produced in the examined region. For that purpose, due to the strong tendency of ultrasonic waves to be diffracted at low frequencies used in classical N.D.T. applications, a high frequency system has been used (Fig. 2).

The main element of the echographic device is the focused transducer. It includes a piezoelectric element, which is damped to obtain a wide band ultrasonic signal with a central frequency of about 40 MHz, and an acoustic lens with a focal length and an angular aperture of 12.7 mm and 2×13.5 deg, respectively. The method has been specially adjusted for detecting deep initiated subsurface cracks. For that purpose, owing to the fact that such cracks roughly grow along the maximum shear stress direction, which is at 45 deg to the normal of the bearing surface, the transducer was tilted by an angle φ of about 20 deg from the normal to the specimen surface (Fig. 3). Indeed, such a configuration of the transducer leads to a direction of the refracted shear wave beam normal to the aforementioned 45 deg cracks and, furthermore, their effective cross section is maximum, which lead to a maximum amplitude for the echo reflected at the crack. Another advantage of this oblique incidence setup is that it reduces the reception of the direct surface echo.

More details on the experimental echographic system used are given elsewhere by Guy et al. (1997), which describes also the initial setup procedure, the measurement accuracy and the results of preliminary experiments for AISI 52100 steel.

Optical and S.E.M. Investigations

Once the fatigue tests had been completed, the disks were cut and suitable cross-sections were examined by optical microscopy and Scanning Electron Microscopy (S.E.M.). In the case of the few tests for which ultrasonic echography had been performed, the cross-sections were chosen in the regions indi-

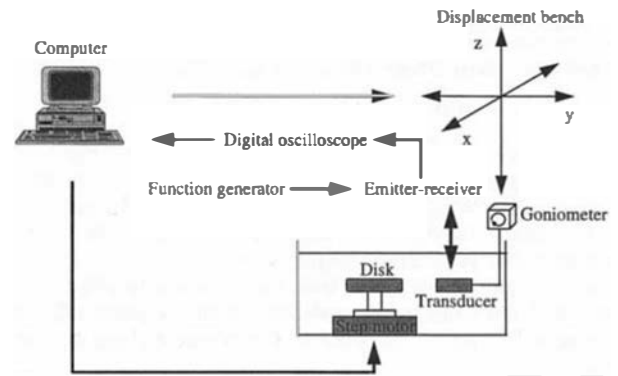


Fig. 2 Schematic of the experimental apparatus for examining a single disk specimen: the raceway is scanned by step by step rotation of the disk and translation of the transducer along the z axis

cated by the ultrasonic spots. In fact, in order to avoid missing the internal reflections that are of very small size, the cut was made close to the position of the ultrasonic indication and then the searched-for inhomogeneity was carefully approached by successive fine polishing of the surface and optical observation, by steps of 10 μm . Once the inhomogeneity was observed satisfactorily, a S.E.M. observation and an E.D.X. (Energy Dispersive X-rays) analysis were carried out, in order to identify the nature of the inhomogeneity responsible for the damage initiation. In other cases for which no ultrasonic echography had been performed, the sub-surface investigations were carried out according to a similar procedure but the cuts were chosen at random.

Test Results for Polished Specimens

Tests with polished surfaces correspond, for these typical operating conditions, to a lambda ratio (lubricant film thickness/composite roughness) larger than 1. Tables A2 and A3 in Appendix A present tests carried out, respectively, at 2.5 and 3.5 GPa, i.e., tests (FM01, FM02, FM05, FM06) and (FH01, FH02, FH05, FH06), respectively. Moreover, since these operating conditions were expected to produce sub-surface initiated damage, two complementary tests with interruptions for high frequency ultrasonic examination have been carried in order to get more information about sub-surface damage initiation. They are tests named FH01bis performed at 3.5 GPa (Table A4), and FXX performed at 4.2 GPa (Table A5), both with M50 disks and under pure rolling condition.

Surface Observation. No surface damage has been observed up to 50×10^6 cycles at 2.5 and 3.5 GPa, whatever the material and the slide-to-roll ratio. However, a sub-surface crack

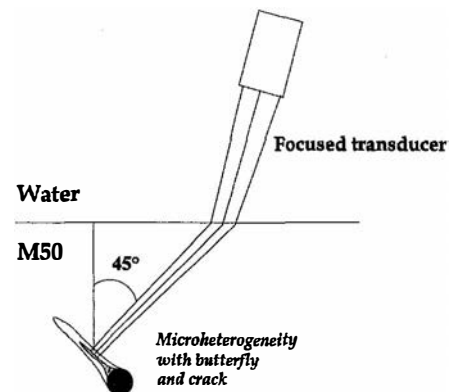


Fig. 3 Principle of oblique incidence echography

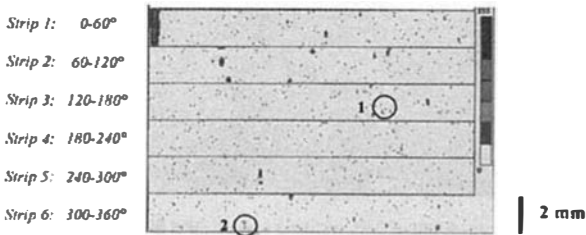


Fig. 4(a) Ultrasonic amplitude image of the whole race in disk M18 prior test. Non-fatigued state: spots 1 and 2 are detected at 260 and 120 μm below the surface, respectively. Each strip represents an angular excursion of 60 deg along the raceway, and a width of 2 mm covering the whole contact raceway.

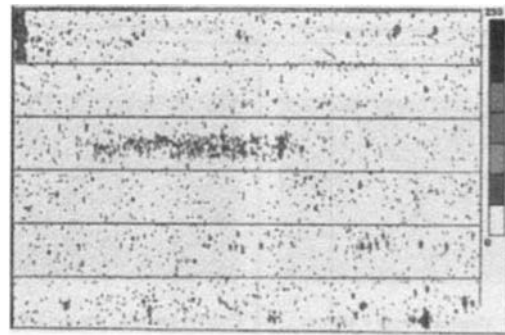


Fig. 4(b) Same as Fig. 4(a) but after 5×10^7 cycles

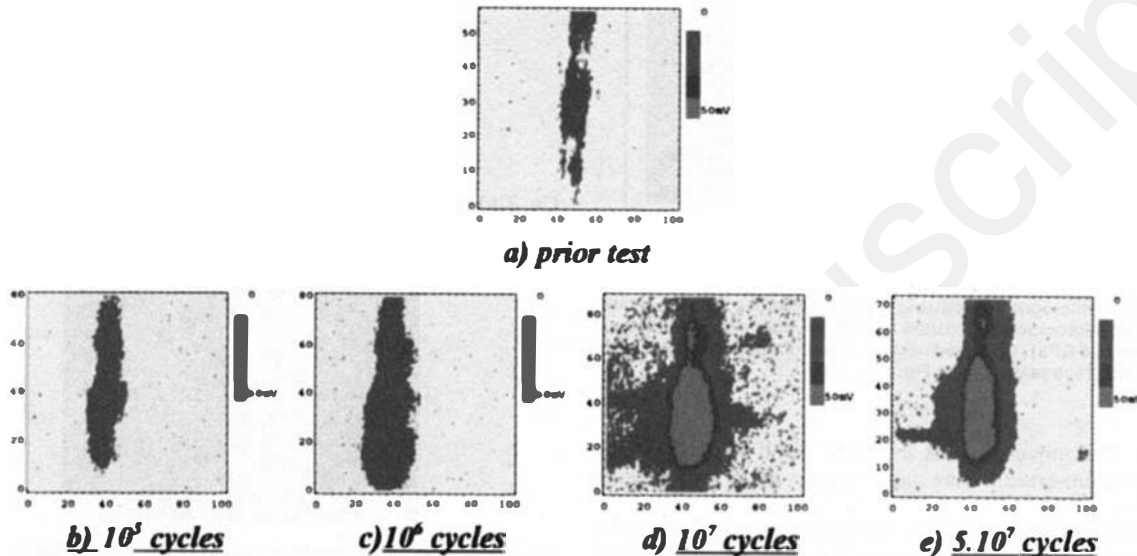


Fig. 4(c) Series of ultrasonic amplitude images of sub-surface reflector no. 2 in disk M18 in mV. Views a, b, c, d, and e corresponding to non-fatigued state, 10^5 , 10^6 , 10^7 , and 5×10^7 cycles, respectively. (Scales are given in number of motor steps; horizontal scale: 1 step = 0.01 deg corresponding to 7 μm along the raceway; vertical scale: 1 step = 10 μm .)

initiated at the Hertzian depth—for the test at 4.2 GPa—has propagated up to the surface, thus leading to a deep spall after 57×10^6 cycles.

Ultrasonic Echography. A first echographic analysis was performed prior to testing for both disk specimens. An example of ultrasonic amplitude image of the whole race of a disk (ref. M18 prior test FH01bis) tested at 3.5 GPa is given in Fig. 4(a). From this image, echoes 1 and 2 located at a depth of 260 and 120 μm , respectively, were thus selected to be investigated in detail throughout the fatigue test. A corresponding series of local images is shown in Fig. 4(c) for spot 2. From this series, it appears clearly that the maximal amplitude recorded for this echo begins to increase as soon as 10^5 cycles have been reached. Then, following further cycling, the maximal amplitude goes on increasing. However, it should be noted that the maximal amplitude of this spot tends to decrease after 5×10^7 cycles. This overall behavior is typical of what has been revealed by ultrasonic investigations. However, somewhat different evolutions were also observed. Especially, many spots which were not detected in the initial state appeared after 5×10^6 cycles, or more. This is best illustrated in Fig. 4(b) that shows an ultrasonic image of the whole disk M18 after 5×10^7 cycles. Moreover, some spots did not exhibit any amplitude decrease subsequent to 5×10^7 cycles.

From the optical and S.E.M. observations of the sub-surface area, which are described in details in the next section, the typical ultrasonic results can be interpreted as follows. The detected echoes correspond to non-metallic inclusions or micro-

cracks (nucleated at non-metallic inclusions or primary carbides) when they are observed in the initial state or subsequent to fatigue, respectively. Hence, the first marked increase in the amplitude of a spot can be associated with crack nucleation. Besides, the amplitude decrease for some echoes subsequent to high number of cycles could be due to the effect of compressive residual stresses which appear in the Hertzian area (Voskamp, 1985) and therefore tend to close the crack faces. Furthermore, the differences that are observed around the typical behavior shown in Fig. 4(c) are linked to the inclusion size, nature, and position below the contact.

Finally, from these investigations, the main contribution to RCF understanding is that many microcracks are nucleated very early in the fatigue life (as soon as 5×10^5 cycles for some of them) but most of them do not propagate out of the area influenced by the inclusion at which they have been nucleated.

Sub-Surface Optical and S.E.M. Investigation. The sub-surface damage frequency is strongly linked with the concentration of inhomogeneities and the load level. Thus, a lot of butterflies and micro-cracks appear around primary carbides in M50 steel at 3.5 GPa. Butterflies and micro-cracks are also observed surrounding non-metallic inclusions both in AISI 52100 and M50 steels, but they are few in number due to the high cleanliness of the materials. Figure 5 presents some butterflies and micro-cracks surrounding non-metallic (such as alumina and calcium aluminate) and metallic (mainly carbide) inclusions in AISI 52100 and M50 steels. The inclination of the butterfly wings and micro-cracks is related to the rolling direction (oppo-

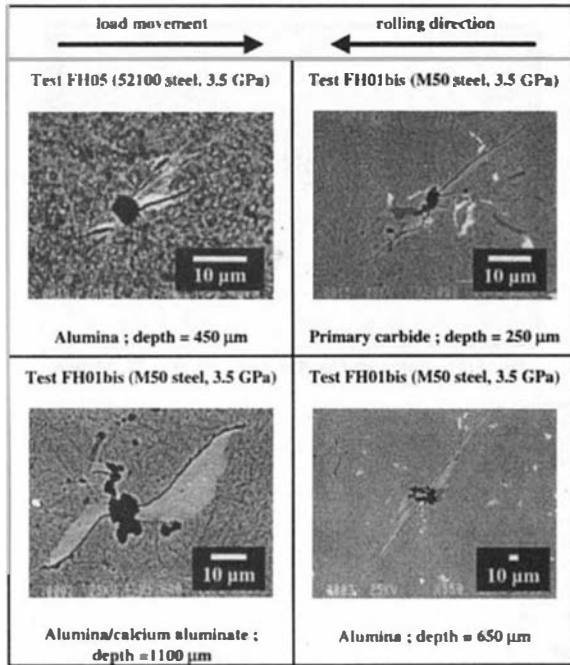


Fig. 5 S.E.M. micrographs showing typical inclusions and associated butterfly and microcrack in polished specimens after contact fatigue (5×10^7 cycles, 3.5 GPa). Observed sections were cut perpendicular to the specimen axis (see plane xOy in Fig. 1).

site to the load movement). It should be noted that such butterflies and micro-cracks were never observed in non-fatigued specimens.

Butterflies and related micro-cracks presented in Fig. 5 have been observed far from the surface. However, an investigation of the butterfly concentration versus depth has been carried out for M50 fatigued specimen after 50×10^6 cycles at 3.5 GPa under pure rolling conditions (a similar investigation for 52100 steel is difficult since the number of initiating sites is too low to perform a statistical approach in one specimen of this material). For that purpose, the sub-surface area has been observed carefully by layers of $100 \mu\text{m}$ in depth, and the number of butterflies per layer has been counted over a surface of about 25 mm^2 . The corresponding histogram is shown in Fig. 6, as well as the histogram giving the number of echoes in percentage. As one can see, we have a reasonable agreement between the statistical distribution of butterflies and the echo frequency versus depth. However, it appears that the depth of maximum concentration of butterflies (between 200 and $300 \mu\text{m}$) is smaller than the depth of the maximum Hertzian shear stress ($457 \mu\text{m}$), which is not clearly understood.

The size of butterfly wings for the test at 4.2 GPa with M50 specimens is generally greater than that observed for tests at

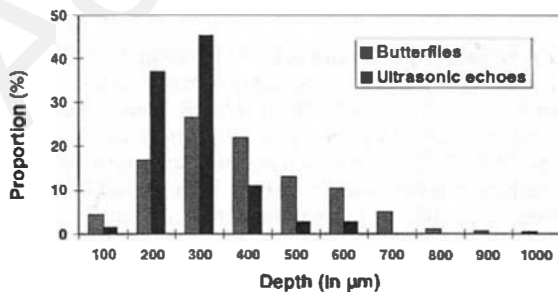


Fig. 6 Butterfly and echo concentrations versus depth for polished specimens at 3.5 GPa under pure rolling condition

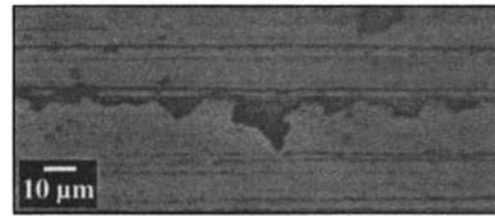


Fig. 7(a) Micro-spalls along grinding marks; AISI 52100 steel; pure rolling; 3.5 GPa, 5×10^7 cycles



Fig. 7(b) Micro-spalls on the top of longitudinal roughness of large wavelength; AISI 52100 steel; pure rolling; 2.5 GPa, 5×10^6 cycles

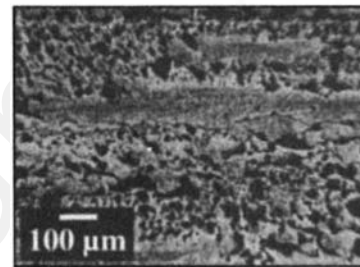


Fig. 7(c) Micro-spalls and longitudinal cracks; M50 steel; pure rolling; 3.5 GPa, 5×10^7 cycles

lower Hertzian pressure. At the same time, cracks are more difficult to detect, i.e., echoes become weaker when the number of cycles increases. This may be explained again by the action of the compressive residual stresses which tend to close both the crack faces and the free space between inclusions and the matrix. Finally, except for the test at 4.2 GPa, no crack extending outside the butterflies has been observed, which means that only crack initiation has occurred under the loading conditions and the number of cycles investigated in this work.

Test Results for Unpolished Specimens

Tests with unpolished surfaces correspond, for these operating conditions, to a lambda ratio (lubricant film thickness/

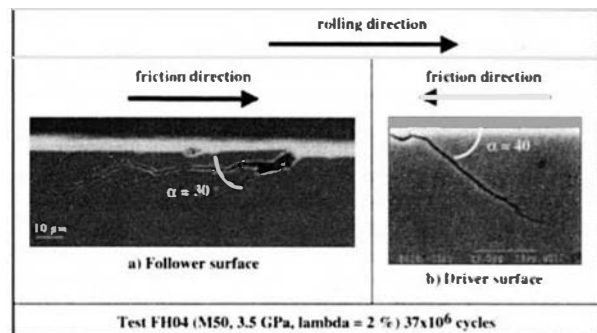


Fig. 8 Micro-crack orientation under rolling plus sliding conditions. Observed sections were cut perpendicular to the specimen axis (see plane xOy in Fig. 1)

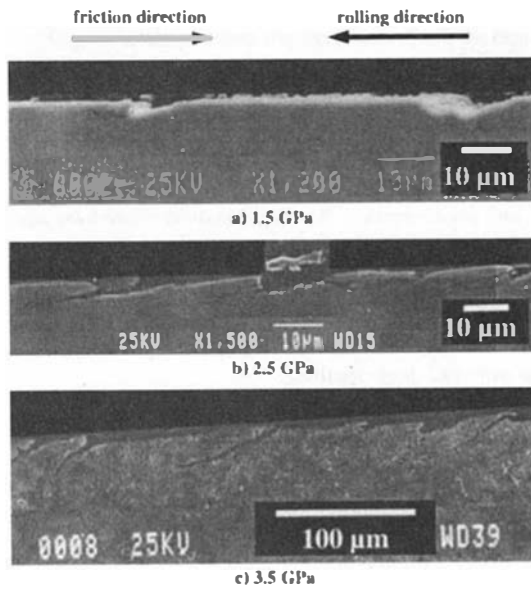


Fig. 9 Longitudinal cut of rolling/sliding micro-spalls in M50 steel

composite roughness) smaller than 1. Tests performed at 1.5, 2.5, and 3.5 GPa are listed in Appendix A in Table A1 (tests FL03, FL04, FL07, and FL08), A2 (tests FM03, FM04, FM07, and FM08), and A3 (tests FH03, FH04, FH07, and FH08), respectively. A complementary test carried out at 3.5 GPa and followed by ultrasonic echography is also presented in Table A4 (test FH03bis).

Surface Observation. Surface distress—which occurrence depends on the roughness amplitude—was always observed for unpolished specimens, independently of the normal load (i.e., at 1.5, 2.5, and 3.5 GPa). It is made of a large population of asperity-scale micro-cracks and micro-spalls which are different depending on the sliding conditions. As shown in Fig. 7(a), pure rolling generates mainly narrow micro-spalls along grinding marks or on the top of longitudinal roughness of large wavelength (Fig. 7(b)). Their depth is limited to 5 to 10 μm . The formation of longitudinal cracks may also be observed after 50×10^6 cycles (Fig. 7(c)). Meanwhile rolling plus sliding produces larger micro-spalls together with transverse micro-cracks. Transverse micro-cracks observed on the surface for rolling plus sliding conditions propagate at an angle of 30 to 40 deg downward away from the direction of the friction direction (Fig. 8), to form micro-spalls. Their depth depends on the normal loading (Fig. 9) and the location on the driver or driven surface. As shown in Fig. 9, the surface micro-crack length for driven surfaces increases strongly with the normal load. Thus, they may reach the Hertzian maximum depth and form a surface initiated deep spall (see Fig. 10 for test at 3.5 GPa), while micro-cracks are not deeper than 10 μm on the driver disk.

Ultrasonic Echography. The ultrasonic examination carried out during test FH03bis has been strongly disturbed by surface damage occurrence. This can be seen by comparing the ultrasonic image of the overall race of an unpolished specimen obtained subsequently to 5×10^7 cycles at 3.5 GPa (Fig. 11(a)) with that one recorded for a smooth specimen at the same number of fatigue cycles (Fig. 4(b)). The former image is completely covered of ultrasonic spots. Moreover, the time analysis of the corresponding echoes shows that most of these echoes originate from the surface, i.e., they are due to surface micro-cracks and micro-spalls.

So, in order to overcome this obstacle, the imaging procedure was slightly modified. A time selection gate has been intro-

duced, thus excluding the echoes whose time of flight corresponds to the transducer/surface back and forth travel. Then, the subsisting echoes are only those reflected from the sub-surface area. The overall image obtained by means of this procedure is given in Fig. 11(b) and the detailed image of a particular spot is given in Fig. 11(c).

Using this method enabled us to follow the evolution of sub-surface damage (i.e., far from the surface). It should be noted that this evaluation can only be qualitative since the amplitude of the waves transmitted at the water/surface interface is significantly disturbed by ultrasonic wave scattering at surface defects. Despite these difficulties, this investigation has shown that the stage of crack initiation at the Hertzian depth is quite similar (number of cycles to occur, concentration of crack nucleation sites) for contact between smooth surfaces and those between rough surfaces.

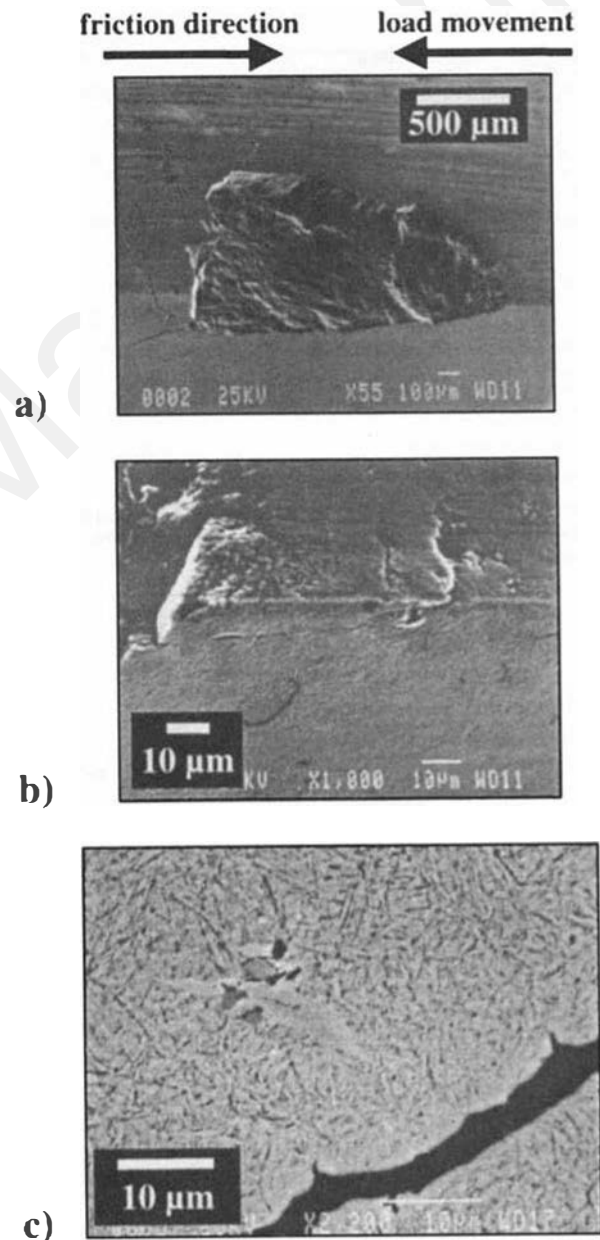


Fig. 10 Surface initiated deep spalling at surface distress (test FH04 after 37×10^6 cycles, follower disk, M50 steel, polished surfaces, 3.5 GPa, slide to roll ratio of 2%). (a) General view (perspective along longitudinal view); (b) zoom on the right side of the spall (perspective view); (c) S.E.M. view of carbide and butterfly in the vicinity of the macro-crack

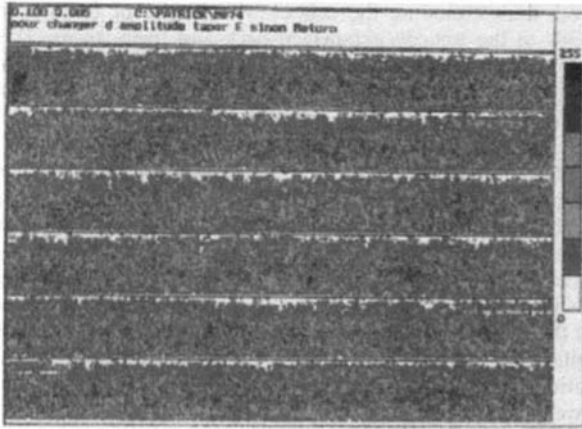


Fig. 11(a) Ultrasonic amplitude image of the whole race in disk M87 of test FH03bis subsequently to 5×10^7 cycles at 3.5 GPa (unpolished surface)

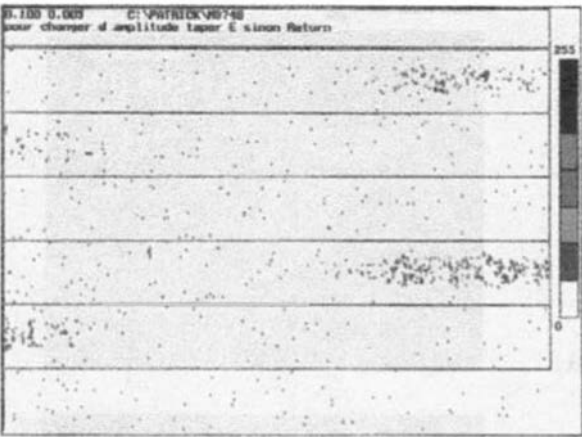


Fig. 11(b) Ultrasonic amplitude image of the whole race in disk M87 of test FH03bis; same conditions as a) but with a time gate selection excluding the surface echoes

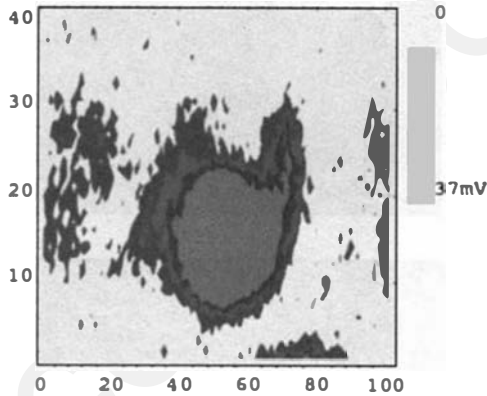


Fig. 11(c) Detailed image of a sub-surface reflector in disk M87 of test FH03bis subsequently to 5×10^7 cycles; measured depth = 250 μm

Sub-Surface Optical and S.E.M. Investigation. These observations confirm the information given by the ultrasonic tests, that is many butterflies and micro-cracks are observed in the sub-surface area, especially in the depth range 200–400 μm , as for polished specimens. However, some butterflies and micro-cracks situated in the range 0–100 μm are also observed. This is best illustrated in Fig. 12 both for AISI 52100 and M50 steels. In the former case, the micro-heterogeneity responsible for the butterfly/micro-crack system has been identified to a titanium nitride (Fig. 12(a)) or to an alumina inclusion (Fig. 12(b)),

whereas in the latter case a primary carbide has been found at the origin of the butterfly/micro-crack system (Fig. 12(c)).

Summary of Observed Fatigue Damage

Surface distress that has been observed for unpolished surfaces is made of a large population of asperity-scale micro-spalls and micro-cracks. A discrimination should be made between the surface distress observed under pure rolling conditions (without transverse micro-cracks) and that observed under rolling/sliding conditions. Surface distress represents a potential failure mode as it modifies the profiles of the contacting surfaces and also can generate other surface failure modes as surface initiated deep spalling.

Surface initiated deep spalling has been observed under rolling plus sliding conditions, for the follower disk in M50 steel at 3.5 GPa after 37×10^6 cycles (test FH04). Optical and S.E.M. examinations of the longitudinal cuts across this macro-spall (Fig. 10) have shown that the deep spall has been originated from the surface distress.

Sub-surface initiated deep spalling has been observed during our experiment FXX after 57×10^6 cycles at 4.2 GPa under pure rolling and for M50 steel. Optical and S.E.M. examinations of the longitudinal cuts across this macro-spall have shown that the deep spall has been originated from a primary carbide located at the Hertzian depth.

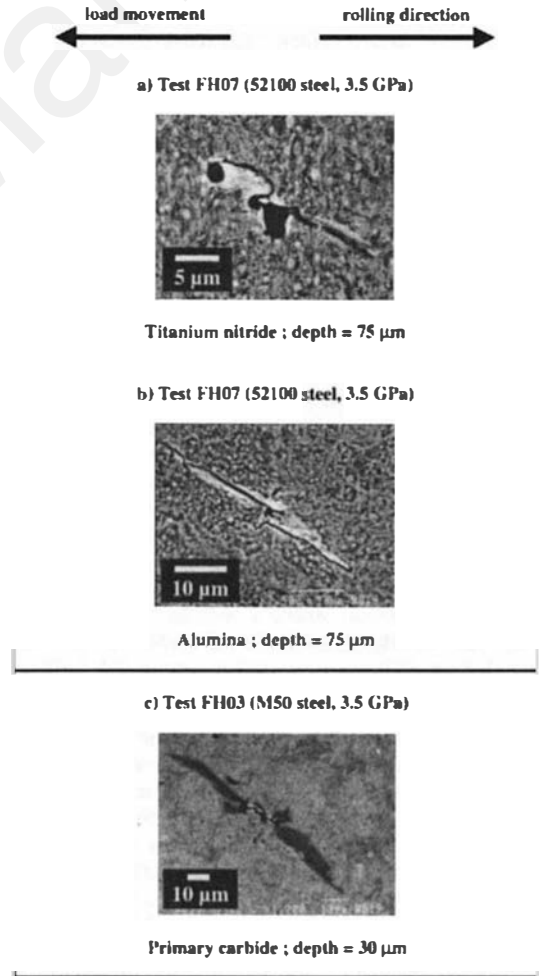


Fig. 12 Sub-surface S.E.M. observations for unpolished specimens at 3.5 GPa. Observed sections were cut perpendicular to the specimen axis (see plane xOy in Fig. 1)

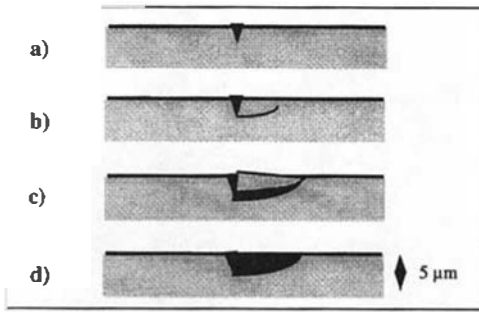


Fig. 13(a) Schematic stages of micro-spall formation along grinding marks (transverse cut), see also Fig. 7(a)

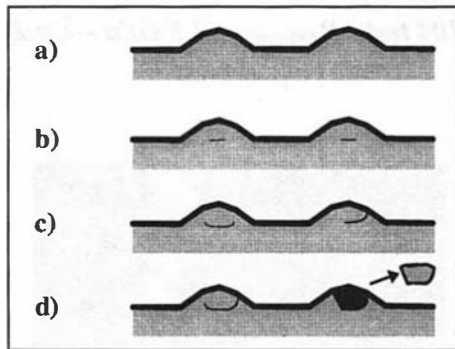


Fig. 13(b) Schematic stages of micro-spall formation below longitudinal roughness of large wavelength (transverse cut), see also Fig. 7(b)

Discussion on Crack Initiation and Growth and Important Parameters

The results of our experimental observations, together with those of some numerical investigations performed in parallel (see Lamagnère, 1996; Dumont, 1997; and Champiot, 1997), have yielded the following comments.

Initiation of Inclusion Originated Fatigue. Initiation and propagation of inclusion originated cracks is the main mode of sub-surface originated fatigue in rolling bearings. Such crack initiation is explained as follows, from various papers devoted to modeling this process (Moreira de Freitas et al., 1983; Champaud, 1988; Vincent et al., 1997). Under the action of the contact stress field, a stress concentration is built up around inhomogeneities (inclusions and primary carbides) due to the elasto-plastic strain mismatch between these inhomogeneities and the martensitic matrix. Once the yield stress of the matrix is reached, a plastic strain is induced in a small domain surrounding the inhomogeneity. Under the repeated action of the contact, dislocations move back and forth and accumulate in this domain. This process often leads to localized changes in the steel microstructure—i.e., white etching area (W.E.A.) with the appearance of butterfly wings—and a crack is nucleated in this domain once a critical density is reached. The number of cycles to crack nucleation versus inhomogeneity properties and operating conditions can thus be predicted from such modeling based on a physical metallurgy approach of RCF (Vincent et al., 1997).

Initiation of Surface Micro-Cracks. Geometrical discontinuities which remain after running-in, such as the bottom end of grinding marks (Fig. 7(a)) and the micro-Hertzian volume below roughness of large wavelength (Fig. 7(b)) or indent ridges, are preferential sites for micro-crack initiation. Micro-cracks propagate parallel to the surface at a few μm depth along the machining direction, leading to the formation of micro-spalls. These processes, which are mainly observed under pure

rolling but seem also to coexist under rolling plus sliding, are schematically shown in Fig. 13(a) and 13(b). However, the number of cycles required to observe the first micro-cracks and subsequent micro-spalls is usually very low (less than 10^5 cycles). Accordingly, the running-in is not always finished and therefore it is an important factor.

Sliding plays also a significant role, as it produces transverse micro-cracks with an angle of 30 to 40 deg opposite to the friction direction. Cracks are located mainly on the top of roughness of large wavelength. The mechanism of crack formation is not yet clearly understood, but some evidence tends to show that the local friction coefficient at the top of asperities may be large enough to initiate transverse micro-cracks. Such micro-cracks are at the origin of micro-spalls, usually wider and deeper than those observed under pure rolling conditions. The different stages of surface distress formation under rolling plus sliding conditions are schematically presented in Fig. 14(a), until a surface initiated deep spall is formed (Fig. 14(b)).

It is not clear whether surface distress occurs under micro-EHL or mixed lubrication regime (with metallic contact between asperities). However, it may appear as soon as the surface asperity amplitude becomes of the same order of magnitude as the lubricant film thickness. Subsequent pressure perturbation on the surface produces some local stress concentrations (i) close to the surface if the local friction coefficient is roughly below 0.3 or (ii) on the surface itself if the local friction coefficient exceeds 0.3 (Dumont, 1997). Initiation is also influenced by surface defects due to machining or mounting, near surface inclusions (Clarke et al., 1985), pollution of the lubricant, contact temperature and sliding velocity. Residual stresses due to machining also play an important role.

Further Initiation and Propagation of Initial Surface Defect. Transient EHL analysis around a surface defect shows that the pressure peak and subsequent high stress concentration is predominant at a location according to the friction direction, that is at the leading edge for driven surfaces and at the trailing edge for driver surfaces (Nélias et al., 1998). This EHL effect depends on the mean contact pressure and whether the lubricant reaches its glassy or quasi-solid state, which is usually the case even at low or moderate normal pressure. That contributes to explain why existing surface distress (micro-cracks and micro-spalls) tends to initiate further micro-cracks and to propagate in the friction direction.

Propagation of Inclusion Originated Micro-Cracks. The main parameters affecting propagation of inclusion originated micro-cracks are the size and nature of inclusions, which define the initial size of the micro-cracks. Two factors may help to further propagate micro-cracks from or toward the surface:

—The attraction of a micro-crack by the closest inclusion (Fig. 15). However this attraction, which occurs in an area limited to the inclusion vicinity (i.e., to a distance up to a few times the inclusion radius), may also be repulsed by the inclusion itself depending on the relative position and orientation of the micro-crack (Champiot, 1997).

—The superposition of stress fields corresponding to different roughness wavelengths that are predominant. This may build a stress bridge linking the near surface area and the Hertzian zone.

As a consequence, a sub-surface initiated deep spall may occur. This point is schematically illustrated in Fig. 16 where the competition between surface and sub-surface crack growth is shown. Sub-surface initiated deep spalling occurs at high normal load and mainly under good elastohydrodynamic conditions, i.e., when the lubricant is abundant and surfaces are smooth. Thus, the crack nucleation takes place at the Hertzian depth around inhomogeneities where the cyclic shear stress is maximum, and the crack propagation occurs towards the sur-

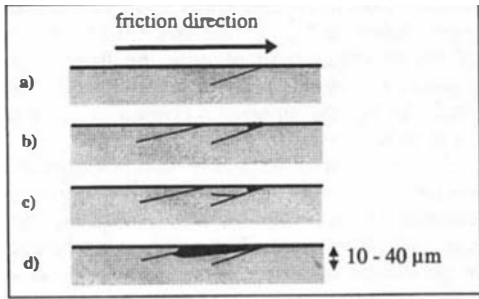


Fig. 14(a) Schematic stages of micro-crack and micro-spall formation under rolling plus sliding (longitudinal cut)

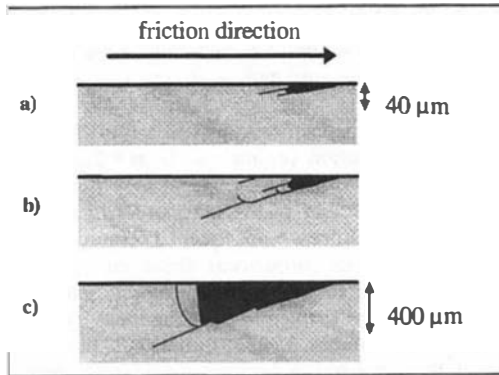


Fig. 14(b) Schematic stages of a surface initiated deep spall (longitudinal cut)

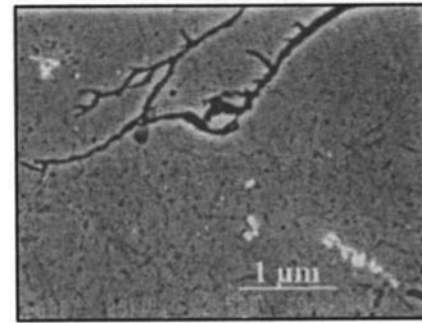
face. It should be noted that the propagation phase is greatly influenced by the stress level and the inclusion frequency within the contacting bodies.

Propagation of Surface or Near Surface Originated Micro-Cracks. As for the propagation of inclusion originated cracks, a roughness composed of undulations of different sizes may build a stress bridge linking the surface and the Hertzian zone through the quiescent zone which does not exist anymore. However, the role of the lubricant by the effect of the hydraulic pressure seems to be more important when a small quantity of oil is entrapped into a crack. Kaneta and Murakami (1991) have numerically shown that in some cases the crack lips may be closed when the load is passing above the crack. The worst situation in regard to the crack propagation occurs when this was preceded by the entrance of oil into the crack that is then entrapped. This contributes to propagate the crack by mode I. This worst combination of crack inclination, load movement, and friction direction is exactly the situation where transverse cracks are found on the driven surfaces. Finally, it should be mentioned that the lubricant viscosity and additives which act (i) on the oil flow from/into a crack and (ii) on the crack face oxidation and then friction coefficient, play also a key role on the surface crack propagation.

Micro-crack propagation which takes place from the surface towards the sub-surface may lead to a surface initiated deep spall. Surface traction forces may act to reduce the depth of the 'quiescent' layer. Furthermore, combination between the sliding direction and the fluid action (Bower, 1987) as well as the presence of non-metallic inclusions (Clarke et al., 1985) contribute to increase the risk of deep spalling.

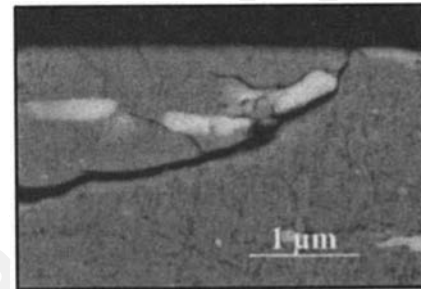
Conclusion

The role of dominant parameters on the rolling contact fatigue of bearing steels can be summarized as follows:



a) Follower disk

(FH04 test - $P_{Hmax} = 3.5 \text{ GPa}$ - $\lambda = 2\%$)



b) Driver disk

(FM04 test - $P_{Hmax} = 2.5 \text{ GPa}$ - $\lambda = 3.5\%$)

Fig. 15 Interactions between micro-cracks and inclusions in M50 steel. Observed sections were cut perpendicular to the specimen axis (see plane xOy in Fig. 1).

Role of Inclusions: They act as stress raisers, leading to localized plastic deformation and crack nucleation, depending on the stress level and the number of cycles. They are at the origin of sub-surface cracks at the Hertzian depth, independently of the roughness quality. They may also be at the origin of

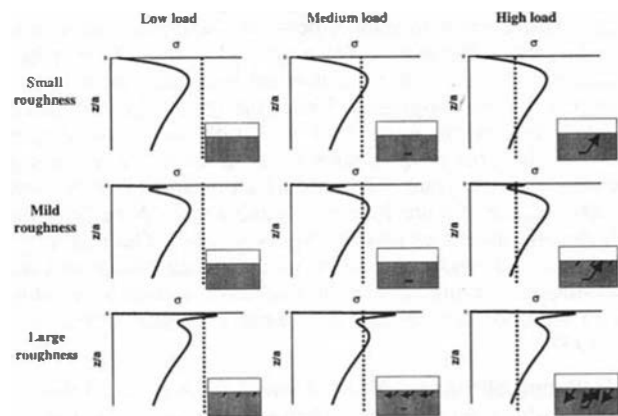


Fig. 16 Competition between surface and subsurface crack growth for different loading and surface roughness. The full line represents the Tresca shear stress σ versus depth z (normalized by the Hertzian pressure and the contact half length a , respectively). The dash line represents the characteristic shear stress below which no crack initiation (straight lines) and propagation (arrow head lines) will occur. This limit takes into account the local inhomogeneities within the material.

near-surface cracks when the roughness produces stress concentration within an important volume near the surface. The oxide type of non-metallic inclusions is much more detrimental than nitride (non-metallic) or carbide (metallic). However, the number of carbides is important in M50 steel. Crack nucleation may be also a consequence of the interaction between several inclusions. Finally the inclusion frequency and distribution is an important factor affecting the crack propagation from or towards the surface, a growing crack being attracted by the neighboring inclusions.

Role of Surface Roughness: Machining marks are at the origin of surface initiated micro-cracks. Large wavelength produces normal pressure fluctuation and sometimes as a consequence the initiation under shear mode of near-surface cracks. The superposition of the Hertzian stress and localized stress due to roughness of large wavelength can create a bridge of stress which may help to propagate cracks from the near surface area or the surface itself to the sub-surface until the Hertzian depth is reached (to form a surface initiated deep spall). The running-in of small wavelength asperities is also of great importance since it produces high stress concentration, even at low normal loads.

Role of Normal Load: The stress level is of course of great importance in the rolling contact fatigue process. Especially, a high load may be very detrimental in the presence of surface distress or other surface damage, as it helps the propagation of near-surface cracks up to the Hertzian depth to form a deep spall, which is a catastrophic failure for a machine element.

Role of Sliding, in Addition to Roughness: Depending on the surface topography and the lubricant thickness, sliding is assumed to be at the origin of the transverse micro-cracks observed on the contacting surface through a local increase of the friction coefficient.

Role of Lubricant: In addition to existing surface micro-cracks and depending on the combination of load movement, friction direction and crack orientation, the lubricant may help to propagate surface cracks by hydraulic pressure effects. The amount of oil entrapped into the crack is linked to the oil flow by the lubricant viscosity. Additives contained in oil may also act on the lubricant fluidity into the crack and then on the hydraulic pressure propagation. They also play a role on the crack face oxidation, which modifies the friction coefficient between the crack faces and then the kinematics of crack propagation. Finally, as shown by transient EHL analysis, the movement of a surface defect produces a stress concentration predominant at a location according to the friction direction. Intensity of stress concentration depends on the mean contact pressure and on the glassy-state transition of the lubricant.

Acknowledgments

This work was developed within the Brite-Euram project "ELABOMM." The authors would like to thank the European Community who supported this research under contract BRE2.CT92.0209. They also gratefully acknowledge the industrial partners of this project for their confidence and their permission to publish this work, i.e., Turboméca, SNECMA, Hispano-Suiza, Renault, SNR from France, MTU, BMW-RR, FAG from Germany, and Rolls-Royce from U.K..

References

Averbach, B., Van Pelt, S., Pearson, P., and Bamberger, E., 1991, "Surface Initiated Spalling Fatigue in M-50 and M50-Nil Bearings," *Lubrication Engineering*, Vol. 47, No. 10, pp. 827-843.

Berthe, D., Michau, B., Flamand, L., and Godet, M., 1978, "Effect of Roughness Ratio and Hertz Pressure on Micro-pits and Spalls in Concentrated Contacts: Theory and Experiments," *Proceedings of 4th Leeds-Lyon Symposium on Tribology*, Lyon, France, 1977, pp. 233-238.

Blake, J. W., and Cheng, H. S., 1991, "A surface pitting Life Model for Spur Gears: Part I-Life Prediction," *ASME JOURNAL OF TRIBOLOGY*, Vol. 113, pp. 712-718.

Bower, A. F., 1988, "The Influence of Crack Face Friction and Trapped Fluid on Surface Initiated Rolling Contact Fatigue Cracks," *ASME JOURNAL OF TRIBOLOGY*, Vol. 110, pp. 704-711.

Champaud, P., 1988, "Contribution à l'étude de la fatigue d'un alliage Fe-Cr (100Cr6) soumis à un champ de contraintes de Hertz. Proposition d'un critère d'amorçage," Ph. D. Thesis, GEMPPM, INSA of Lyon.

Champiot, F., 1997, "Contribution à l'analyse et à la modélisation de la propagation des fissures courtes dans les aciers soumis à la fatigue de roulement," Ph. D. Thesis, GEMPPM, INSA of Lyon.

Cheng, W., Cheng, H. S., and Keer, L. M., 1994a, "Longitudinal Crack Initiation Under Pure Rolling Contact Fatigue," *STLE Tribology Transactions*, Vol. 37, No. 1, pp. 51-58.

Cheng, W., Cheng, H. S., and Keer, L. M., 1994b, "Experimental Investigation on Rolling/Sliding Contact Fatigue Crack Initiation with Artificial Defects," *STLE Tribology Transactions*, Vol. 37, No. 1, pp. 62-73.

Cheng, W., Cheng, H. S., Mura, T., and Keer, L. M., 1994c, "Micromechanics Modeling of Crack Initiation Under Contact Fatigue," *ASME JOURNAL OF TRIBOLOGY*, Vol. 116, pp. 2-8.

Cheng, W., and Cheng, H. S., 1995, "Effect of Surface Roughness Orientation on Pitting Resistance of Lubricated Rollers," *STLE Tribology Transactions*, Vol. 38, No. 2, pp. 396-402.

Cheng, W., and Cheng, H. S., 1997, "Semi-Analytical Modeling of Crack Initiation Dominant Contact Fatigue Life for Roller Bearings," *ASME JOURNAL OF TRIBOLOGY*, Vol. 119, pp. 233-240.

Chiu, Y. P., 1998, "Longitudinal Crack Initiation Under Pure Rolling Contact Fatigue," *STLE Tribology Transactions*, Preprint No. 97-AM-1A-1, Vol. 41.

Clarke, T. R., Miller, G. R., Keer, L. M., and Cheng, H. S., 1985, "The Role of Near-Surface Inclusions in the Pitting of Gears," *ASLE Transactions*, Vol. 28, No. 1, pp. 111-116.

Dumont, M.-L., 1997, "Etude des endommagements de surface induits par la fatigue de roulement dans les contacts élastohydrodynamiques pour des aciers M50 et 100Cr6," Ph. D. thesis, LMC, INSA of Lyon.

Dyson, A., 1975, "Scuffing—A Review," *Tribology International*, Vol. 8, No. 2, pp. 77-87.

Fan, H., Keer, L. M., W. Cheng, and Cheng, H. S., 1993, "Competition Between Fatigue Crack Propagation and Wear," *ASME JOURNAL OF TRIBOLOGY*, Vol. 115, pp. 141-147.

Guy, P., Meynaud, P., Vincent, A., Dufragne, G., and Baudry, G., 1997, "Sub-surface Damage Investigation by High Frequency Ultrasonic Echography on 100Cr6 Bearing Steel," *Tribology International*, Vol. 30, No. 4, pp. 247-259.

Kaneta, M., Yatsuzuka, H., and Murakami, Y., 1985, "Mechanism of Crack Growth in Lubricated Rolling/Sliding Contact," *ASLE Transactions*, Vol. 28, No. 3, pp. 407-414.

Kaneta, M., and Murakami, Y., 1991, "Propagation of Semi-Elliptical Surface Cracks in Lubricated Rolling/Sliding Elliptical Contacts," *ASME JOURNAL OF TRIBOLOGY*, Vol. 113, pp. 270-275.

Keer, L. M., and Bryant, M. D., 1983, "A Pitting Model of Contact Fatigue," *ASME JOURNAL OF LUBRICATION TECHNOLOGY*, Vol. 105, No. 2, pp. 198-205.

Kuo, C. H., Keer, L. M., and Bujold, M. P., 1997, "Effects of Multiple Cracking on Crack Growth and Coalescence in Contact Fatigue," *ASME JOURNAL OF TRIBOLOGY*, Vol. 119, pp. 385-390.

Lamagnère, P., 1996, "Etude et modélisation de l'amorçage des fissures de fatigue de roulement au voisinage des microhétérogénéités dans l'acier M50," Ph. D. thesis, GEMPPM, INSA of Lyon.

Lamagnère, P., Fougères, R., Lorman, G., Girodin, D., Dufragne, G., Vergne, F., and Vincent, A., 1998, "A Physically Based Model for Endurance Limit of Bearing Steels," *ASME JOURNAL OF TRIBOLOGY*, Vol. 120, pp. 421-426.

Lee, J. K., and Keer, L. M., 1986, "Study of a Three-Dimensional Crack Terminating at an Interface," *ASME Journal of Applied Mechanics*, Vol. 108, pp. 316-331.

Lee, J. K., and Mal, A. K., 1997, "A Volume Integral Equation Technique for Multiple Inclusion and Crack Interaction Problems," *ASME Journal of Applied Mechanics*, Vol. 119, pp. 23-31.

Littmann, W. E., and Widner, R. L., 1966, "Propagation of Contact Fatigue from Surface and Subsurface Origins," *ASME Journal of Basic Engineering*, pp. 624-636.

Littmann, W. E., and Widner, R. L., Wolfe, J. O., and Stover, J. D., 1968, "The Role of Lubrication in the Propagation of Contact Fatigue Cracks," *ASME JOURNAL OF LUBRICATION TECHNOLOGY*, Vol. 90, pp. 89-100.

Littmann, W. E., 1970, "The Mechanism of Contact Fatigue," *Interdisciplinary Approach to the Lubrication of Concentrated Contacts*, NASA SP-237, pp. 309-377.

Lundberg, G., and Palmgren, A., 1947, "Dynamic Capacity of Rolling Bearings," *Acta Polytechnica 7*, Mech. Engr. Series, Vol. 1, No. 3, Stockholm, Sweden.

Martin, J. A., and Eberhardt, A. D., 1967, "Identification of Potential Failure Nuclei in Rolling Contact Fatigue," *ASME Journal of Basic Engineering*, pp. 932-942.

Matsuo, K., Seki, M., Shirahama, S., Miyajima, M., and Yamada, H., 1994, "Influence of Lubricants on Rolling Contact Fatigue," *Japanese Journal of Tribology*, Vol. 39, No. 8, pp. 981-994.

Meynaud, P., 1995a, "Prévision de la durée de vie en fatigue de roulement d'un acier à partir de ses caractéristiques élastoplastiques et de celles de ses inclusions," Ph. D. Thesis, GEMPPM, INSA of Lyon.

Meynaud, P., Lormand, G., Vincent, A., Fougères, R., Baudry, G., Saleil, J., Girodin, D., and Dudragne, G., 1995b, "Statistical Approach of Bearing Fatigue Life Time," *Proceedings of the 2nd International Symposium on Bearing Steels*, Arles, France, June 6–9, 1995.

Moreira de Freitas, M., and François, D., 1983, "Formation de phase blanche en fatigue de roulement," *Scripta Metallurgica*, Vol. 17, pp. 683–686.

Mura, T., and Tanaka, K., 1981, "Dislocation Dipole Models for Fatigue Crack Initiation," *Mechanics of Fatigue*, T. Mura, ed., ASME AMD, Vol. 47, pp. 111–131.

Mura, T., and Nakasone, Y., 1990, "A Theory of Fatigue Crack Initiation in Solids," *ASME Journal of Applied Mechanics*, Vol. 57, pp. 1–6.

Murakami, Y., Kaneta, M., and Yatsuzuka, H., 1985, "Analysis of Surface Crack Propagation in Lubricated Rolling Contact," *ASLE Transactions*, Vol. 28, No. 1, pp. 60–68.

Murakami, Y., Sakae, C., and Ichimaru, K., 1994, "Three-Dimensional Fracture Mechanics Analysis of Pit Formation Mechanism Under Lubricated Rolling-Sliding Contact Loading," *STLE Tribology Transactions*, Vol. 37, No. 3, pp. 445–454.

Nélias, D., Dumont, M.-L., Couhier, F., Dudragne, G., and Flaman, L., 1998, "Experimental and Theoretical Investigation on Rolling Contact Fatigue of 52100 and M50 Steels Under EHL or Micro-EHL Conditions," *ASME JOURNAL OF TRIBOLOGY*, Preprint No. 97-Trib-7, Vol. 120, pp. 184–190.

Rocher, S., 1994, "Contribution à l'analyse et la modélisation de la propagation des fissures courtes dans l'acier 100Cr6 soumis à la fatigue de roulement," Ph. D. thesis, GEMPPM, INSA of Lyon.

Sanchette-Gosset, L., 1993, "Contribution à l'analyse et à la modélisation de l'amorçage des fissures dans l'acier 100Cr6 soumis à la fatigue de roulement," Ph. D. thesis, GEMPPM, INSA of Lyon.

Shibata, M., Yoshida, A., Aihara, S., Nitani, A., and Tsushima, N., 1994, "Effects of Various Factors on the Rolling Contact Fatigue," *Japanese Journal of Tribology*, Vol. 36, No. 8, pp. 963–979.

Soeta, N., and Yamamoto, T., 1982, "Effect of Tangential Traction and Roughness on Crack Initiation/Propagation During Rolling Contact," *ASLE Transactions*, Vol. 25, pp. 198–206.

Sushchenko, S. A., 1997, "Photoelastic Analysis of Stress Concentrations in a Two-Dimensional Model of Hard Inclusions in a Metal Matrix," *STLE Tribology Transactions*, Vol. 40, No. 2, pp. 386–390.

Tallian, T. E., Chiu, Y. P., and Amerongen, E. V., 1978, "Prediction of Traction and Microgeometry Effects on Rolling Contact Fatigue Life," *ASME JOURNAL OF LUBRICATION TECHNOLOGY*, Vol. 100, No. 2, pp. 156–166.

Tallian, T. E., 1992, *Failure Atlas for Hertz Contact Machine Elements*, ASME Press, New York.

Tanaka, K., and Mura, T., 1982, "A Theory of Fatigue Crack Initiation at Inclusions," *Metallurgical Trans. A*, Vol. 13A, pp. 117–123.

Vergne, P., and Nélias, D., 1996, "Tribological and Rheological Properties of a MIL-L-23699 Lubricant," *Proceedings of the International Tribology Conference*, Yokohama, Japan, 1995, Vol. 2, pp. 691–696.

Vincent, A., Lormand, G., Fougères, R., Gosset, L., Girodin, D., and Dudragne, G., 1995, "Modelling Shape and Size of White Etching Areas Formed Around Inclusions in Bearing Steels under Rolling Contact Fatigue," *Proceedings of the 2nd International Symposium on Bearing Steels*, Arles, France, June 6–9, 1995.

Vincent, A., Lormand, G., Lamagnère, P., Gosset, L., Girodin, D., Dudragne, G., and Fougères, R., 1997, "From White Etching Areas Formed Around Inclusions to Crack Nucleation in Bearing Steels under Rolling Contact Fatigue," *Proceedings of Symposium on "Bearing Steels: Into the 21st Century"*, ASTM STP 1327.

Voskamp, A. P., 1985, "Material Response to Rolling Contact Loading," *ASME JOURNAL OF TRIBOLOGY*, Vol. 107, pp. 359–366.

Way, S., 1935, "Pitting Due to Rolling Contact," *ASME Journal of Applied Mechanics*, Vol. 2, pp. A49–A58.

Yoshioka, T., and Fujiwara, T., 1988, "Measurement of Propagation Initiation and Propagation Time of Rolling Contact Fatigue Cracks by Observation of Acoustic Emission and Vibration," *Interface Dynamics*, Dowson D., Taylor C., Godet M. and Berthe D. eds., Elsevier, Amsterdam, pp. 29–33.

Yoshioka, T., 1993, "Detection of Rolling Contact Sub-Surface Fatigue Cracks Using Acoustic Emission Technique," *Lubrication Engineering*, Vol. 49, No. 4, pp. 303–308.

Yoshioka, T., and Takeida, M., 1995, "Clarification of Rolling Contact Fatigue Initiation Using Acoustic Emission Technique," *Lubrication Engineering*, Vol. 51, No. 1, pp. 41–44.

Zhou, R. S., Cheng, H. S., and Mura, T., 1989, "Micropitting in Rolling and Sliding Contact Under Mixed Lubrication," *ASME JOURNAL OF TRIBOLOGY*, Vol. 111, pp. 605–613.

APPENDIX A

Test List, and Corresponding Operating Conditions and Fatigue Damage

Table A1 Operating conditions and corresponding types of fatigue damage observed at 1.5 GPa

| Tests | Material | h_r/σ | Slide to roll ratio | Max nb of cycles | Observations at the end of the test |
|-------|----------|--------------|---------------------|-------------------------|--|
| FL03 | M50 | 0.719 | 0% | 20×10^6 cycles | surface distress/no sub-surface damage |
| FL04 | M50 | 0.667 | 6% | 10×10^6 cycles | surface distress/no sub-surface damage |
| FL07 | 52100 | 0.776 | 0% | 20×10^6 cycles | surface distress/no sub-surface damage |
| FL08 | 52100 | 0.790 | 6% | 10×10^6 cycles | surface distress/no sub-surface damage |

Table A2 Operating conditions and corresponding types of fatigue damage observed at 2.5 GPa

| Tests | Material | h_r/σ | Slide to roll ratio | Max no of cycles | Observations at the end of the test |
|-------|----------|--------------|---------------------|-------------------------|---|
| FM01 | M50 | 1.206 | 0% | 50×10^6 cycles | no surface damage/sub-surface butterflies |
| FM02 | M50 | 1.207 | 3.5% | 50×10^6 cycles | no surface damage/sub-surface butterflies |
| FM03 | M50 | 0.582 | 0% | 20×10^6 cycles | surface distress/sub-surface butterflies |
| FM04 | M50 | 0.479 | 3.5% | 10×10^6 cycles | surface distress/sub-surface butterflies |
| FM05 | 52100 | 1.305 | 0% | 50×10^6 cycles | no surface damage/sub-surface butterflies |
| FM06 | 52100 | 1.275 | 3.5% | 50×10^6 cycles | no surface damage/sub-surface butterflies |
| FM07 | 52100 | 0.583 | 0% | 20×10^6 cycles | surface distress/sub-surface butterflies |
| FM08 | 52100 | 0.599 | 3.5% | 10×10^6 cycles | surface distress/sub-surface butterflies |

Table A3 Operating conditions and corresponding types of fatigue damage observed at 3.5 GPa

| Tests | Material | h_r/σ | Slide to roll ratio | Max no of cycles | Observations at the end of the test |
|-------|----------|--------------|---------------------|-------------------------|---|
| FH01 | M50 | 1.169 | 0% | 50×10^6 cycles | no surface damage/sub-surface butterflies & μ -cracks |
| FH02 | M50 | 1.237 | 2% | 50×10^6 cycles | no surface damage/sub-surface butterflies & μ -cracks |
| FH03 | M50 | 0.614 | 0% | 50×10^6 cycles | surface distress/sub-surface butterflies & μ -cracks |
| FH04 | M50 | 0.628 | 2% | 37×10^6 cycles | surface distress, one surface origin spall at 37×10^6 cycles/sub-surface butterflies & μ -cracks |
| FH05 | 52100 | 1.445 | 0% | 50×10^6 cycles | no surface damage/sub-surface butterflies & μ -cracks |
| FH06 | 52100 | 1.153 | 2% | 50×10^6 cycles | no surface damage/sub-surface butterflies & μ -cracks |
| FH07 | 52100 | 0.572 | 0% | 50×10^6 cycles | surface distress/sub-surface butterflies & μ -cracks |
| FH08 | 52100 | 0.809 | 2% | 50×10^6 cycles | surface distress/sub-surface butterflies & μ -cracks |

Table A4 List of interrupted tests at 3.5 GPa with ultrasonic echography inspection

| Tests | Material | h_v/σ | Slide to roll ratio | Max no of cycles | Observations at the end of the test |
|---------|----------|--------------|---------------------|-------------------------|---|
| FH01bis | M50 | 1.169 | 0% | 50×10^6 cycles | no surface damage/sub-surface butterflies & μ -cracks |
| FH03bis | M50 | 0.614 | 0% | 50×10^6 cycles | surface distress/sub-surface butterflies & μ -cracks |

Table A5 Operating conditions of interrupted test at 4.2 GPa with ultrasonic echography inspection

| Tests | Material | h_v/σ | Slide to roll ratio | Max no of cycles | Observations at the end of the test |
|-------|----------|--------------|---------------------|-------------------------|---|
| FXX | M50 | 1.247 | 0% | 57×10^6 cycles | one sub-surface origin spall at 57×10^6 cycles/sub-surface butterflies & μ -cracks |

Note: The central lubricant film thickness h_v is given by the well-known Hamrock and Dowson's formula for elliptical point contact.